CDDpress

www.nature.com/cdd

ARTICLE

Check for updates

DNA 5mC and RNA m^{6}A modification successively facilitates the initiation and perpetuation stages of HSC activation in liver fibrosis progression

Yue Feng[1,2], Shihui Guo[1,2], Yulan Zhao[1,2], Haibo Dong[3], Jiayu Qian[2], Yun Hu[4], Lei Wu[1,2], Yimin Jia[1,2] and Ruqian Zhao[1,2]✉

Hepatic stellate cells (HSC) are key effector cells in liver fibrosis. Upon stimulation, the quiescent HSC undergoes complex morphological and functional changes to transdifferentiate into activated collagen-producing myofibroblasts. DNA/RNA methylations (5mC/m^{6}A) are both implicated to participate in hepatic fibrosis, yet their respective roles and specific targets in HSC activation remain elusive. Here, we demonstrate that 5mC is indispensable for the initiation stage of HSC activation (myofibroblast transdifferentiation), whereas m^{6}A is essential for the perpetuation stage of HSC activation (excessive ECM production). Mechanistically, DNA 5mC hypermethylation on the promoter of SOCS3 and PPARγ genes leads to STAT3-mediated metabolic reprogramming and lipid loss in the initiation stage. RNA m^{6}A hypermethylation on the transcripts of major collagen genes enhances the mRNA stability in a YTHDF1-dependent manner, which contributes to massive ECM production. Vitamin A-coupled YTHDF1 siRNA alleviates CCl_4-induced liver fibrosis in mice through HSC-specific inhibition of collagen production. HIF-1α, which is transactivated by STAT3, serves as a bridge linking the initiation and the perpetuation stages through transactivating YTHDF1. These findings indicate successive roles of DNA 5mC and RNA m^{6}A modification in the progression of HSC activation, which provides new drug targets for epigenetic therapy of liver fibrosis.

Cell Death & Differentiation (2023) 30:1211–1220; https://doi.org/10.1038/s41418-023-01130-3

INTRODUCTION

Non-alcoholic fatty liver disease (NAFLD) is the most common chronic liver disease, with an estimated prevalence of 25% worldwide [1]. The NAFLD spectrum consists of the following entities: isolated fatty liver (non-alcoholic fatty liver, NAFL), non-alcoholic steatohepatitis (NASH), liver fibrosis, and cirrhosis that may lead to liver failure or hepatocellular carcinoma (HCC) [2]. Epigenetic modifications, notably DNA 5-methylcytosine (5mC) and mRNA N6-methyladenosine (m^{6}A), are implicated in the pathogenesis of NAFL [3, 4], NASH [4, 5], cirrhosis [6, 7], and HCC [8–10]. However, the changes of these epigenetic modifications and their roles in NAFLD progression have been contradictory, due to complex molecular and cellular heterogeneity in different disease models at different stages.

Liver fibrosis is a critical step in developing cirrhosis [11, 12]. Hepatic stellate cells (HSC) activation plays a crucial role in liver fibrosis and thus serves as a potential drug target for hepatic fibrosis therapy. Transforming growth factor-β1 (TGF-β1), the most potent fibrogenic cytokine [13], is commonly used to activate HSC in vitro. HSC activation comprises two consecutive yet distinct stages; the initiation stage refers to the transdifferentiation of quiescent HSC to myofibroblast-like cells (MFB) with loss of lipid droplets, whereas the perpetuation stage is characterized by excessive extracellular matrix (ECM) production [14, 15].

Increasing evidence has shown that DNA 5mC modifications are involved in cirrhosis and hepatic stellate cells (HSC) activation. *De novo* DNA methylation appears to be indispensable for cirrhosis and HSC activation, as DNA 5mC methyltransferase 3A (DNMT3A) and DNMT3B proteins are significantly increased in cirrhotic liver, and DNMT3A knockdown significantly inhibits HSC activation in vitro [6]. Similarly, DNA methyltransferase inhibitor 5-Aza-2′-deoxycytidine (5-aza) prevents the lipid loss via reversing the epigenetic repression of lipogenic PPARγ gene and thereby inhibits HSC-MFB transdifferentiation [16]. Nevertheless, whether DNA 5mC modification also participates in the perpetuation stage of HSC activation remains unclear.

RNA m^{6}A methylation is the most abundant and highly dynamic modification throughout the transcriptome, which impacts numerous biological processes in health and disease, via regulating almost all aspects of mRNA metabolism including splicing, translation, and stability [17]. RNA methylation has recently been reported to play a regulatory role in liver fibrosis and HSC activation. However, both decrease and increase of m^{6}A modifications are reported in the CCl_4-induced mouse model of liver fibrosis [7, 18]. Recently, efforts have been taken to identify the potential mRNA targets of m^{6}A and related pathways using in vitro model of HSC activation [18–20]. However, no consensus can be reached probably due to the

[1]MOE Joint International Research Laboratory of Animal Health and Food Safety, Nanjing Agricultural University, Nanjing, Jiangsu, PR China. [2]Key Laboratory of Animal Physiology & Biochemistry, College of Veterinary Medicine, Nanjing Agricultural University, Nanjing, Jiangsu, PR China. [3]Center for Translational Biomedical Research, UNCG, Kannapolis, NC, USA. [4]College of Animal Science and Technology, Yangzhou University, Yangzhou, Jiangsu, PR China. ✉email: zhaoruqian@njau.edu.cn

Received: 25 July 2022 Revised: 2 February 2023 Accepted: 9 February 2023
Published online: 25 February 2023

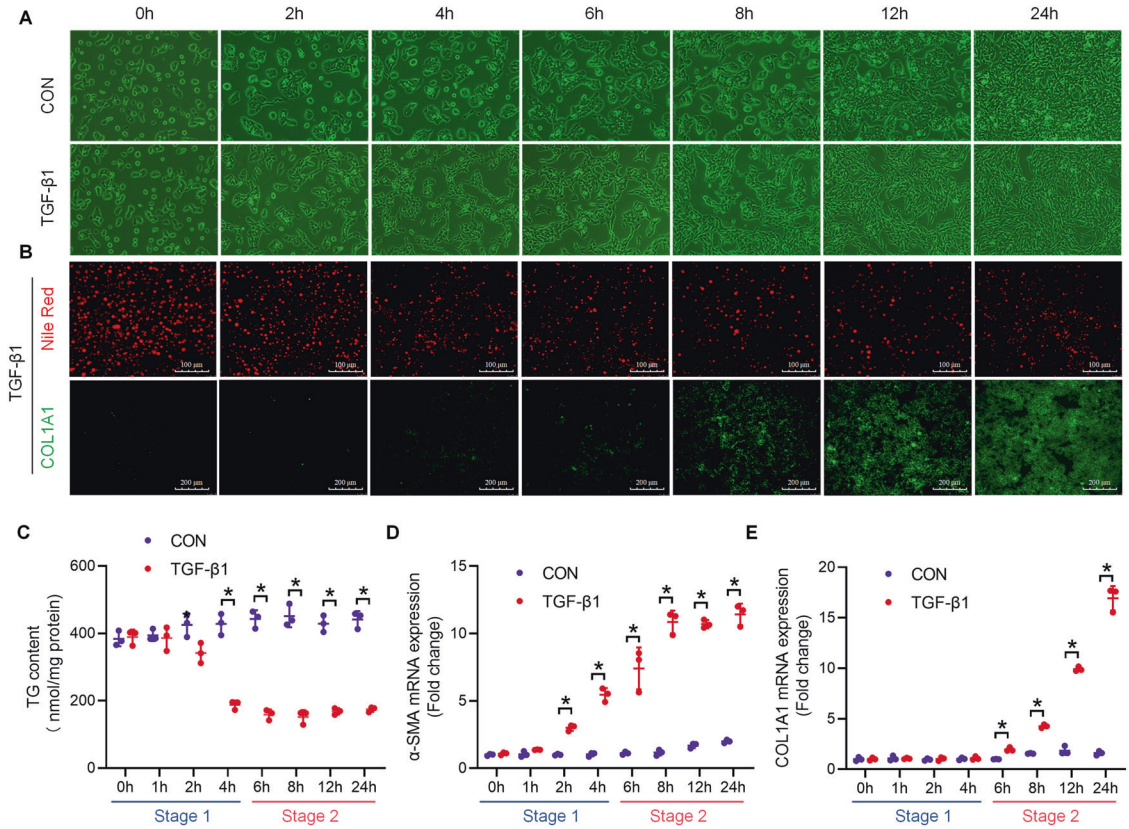

Fig. 1 The time-course analysis characterizes the initiation and perpetuation stages of HSC activation. A Cell morphological changes ($n = 3$). **B** Nile red and COL1A1 immunofluorescence staining ($n = 3$). **C** Intracellular TG content ($n = 3$). **D** α-SMA mRNA expression ($n = 3$). **E** COL1A1 mRNA expression. Stage 1, initiation stage (0–4 h); Stage 2, perpetuation stage (6–24 h). Values are means ± SD, $*p < 0.05$.

complexity of HSC activation involving stage-specific regulatory mechanisms.

In this study, we performed a time-course mapping throughout the process of TGF-β1-induced HSC activation to differentiate the initiation and perpetuation stages, and elucidated the dynamic changes and stage-specific functions of 5mC/m^{6}A methylation during HSC activation. DNA 5mC hypermethylation on the promoter of SOCS3 and PPARγ genes leads to metabolic reprogramming and lipid loss during the initiation stage, and m^{6}A hypermethylation on transcripts of collagen family exacerbates collagen production in a YTHDF1-dependent manner during the perpetuation stage. HSC-specific knockdown of YTHDF1 significantly alleviates CCl_4-induced liver fibrosis in mice. STAT3-activated HIF-1α pathway serves as a bridge linking the initiation stage and the perpetuation stage in HSC activation. These findings elaborate the stage-specific roles of DNA 5mC and RNA m^{6}A modifications in the progression of HSC activation, and provide novel insights for developing targeted therapy for liver fibrosis.

RESULTS

The time-course analysis characterizes the initiation and perpetuation stages of HSC activation

To differentiate the initiation and perpetuation stages of HSC activation, cells were harvested every 2 h from TGF-β1 stimulation throughout the entire process of 24 h for morphological characterization and gene expression analyses. Quiescent HSC transdifferentiate into MFB showing typical spindle or stellate shape within 4 h after TGF-β1 treatment, and maintained MFB morphology thereafter (Fig. 1A). Moreover, loss of lipid droplets (Fig. 1B) and decreased triglyceride (TG) content (Fig. 1C) were observed during this stage, together with increased mRNA expression of α-SMA, a classic marker for MFB (Fig. 1D). Based on these observations, the first 4 h after TGF-β1 treatment was classified as the initiation stage (Stage 1). COL1A1, a key ECM component, was increased at both mRNA and protein levels from 6 to 24 h (Fig. 1B, E), which marks the perpetuation stage of HSC activation (Stage 2).

5mC and m^{6}A modification increases at different stages during HSC activation

To explore the link between epigenetic regulation and HSC activation, total DNA 5mC and RNA m^{6}A levels were dynamically determined throughout the entire process, together with the expression of genes related to DNA and RNA methylation. Global 5mC marks started to increase at 4 h in Stage 1 and maintained high in Stage 2 (Figs. 2A and S1A). Accordantly, an upregulation of DNMT3A was detected initially from 2 to 4 h in Stage 1 at both mRNA (Fig. 2B) and protein (Figs. 2C and S1B) levels. In contrast, global m^{6}A marks started to increase from 6 h onwards in Stage 2 (Figs. 2D and S1C). The same pattern was observed for the expression of METTL3 (Figs. 2E, F and S1D) and METTL14 (Fig. S1E–G). Thus, DNA 5mC and RNA m^{6}A hypermethylation are associated, respectively, with the initiation and perpetuation stage of HSC activation.

5mC and m^{6}A hypermethylation regulates different stages of HSC activation

To verify the effect of 5mC on HSC activation, cells were treated with specific 5mC inhibitor 5-aza in different stages of activation (Fig. S1H). 5-aza administered 12 h prior to TGF-β1 stimulation completely prevented the decrease of TG content (Fig. 2G) and the loss of lipid droplets (Fig. 2H) in Stage 1. Consequently,

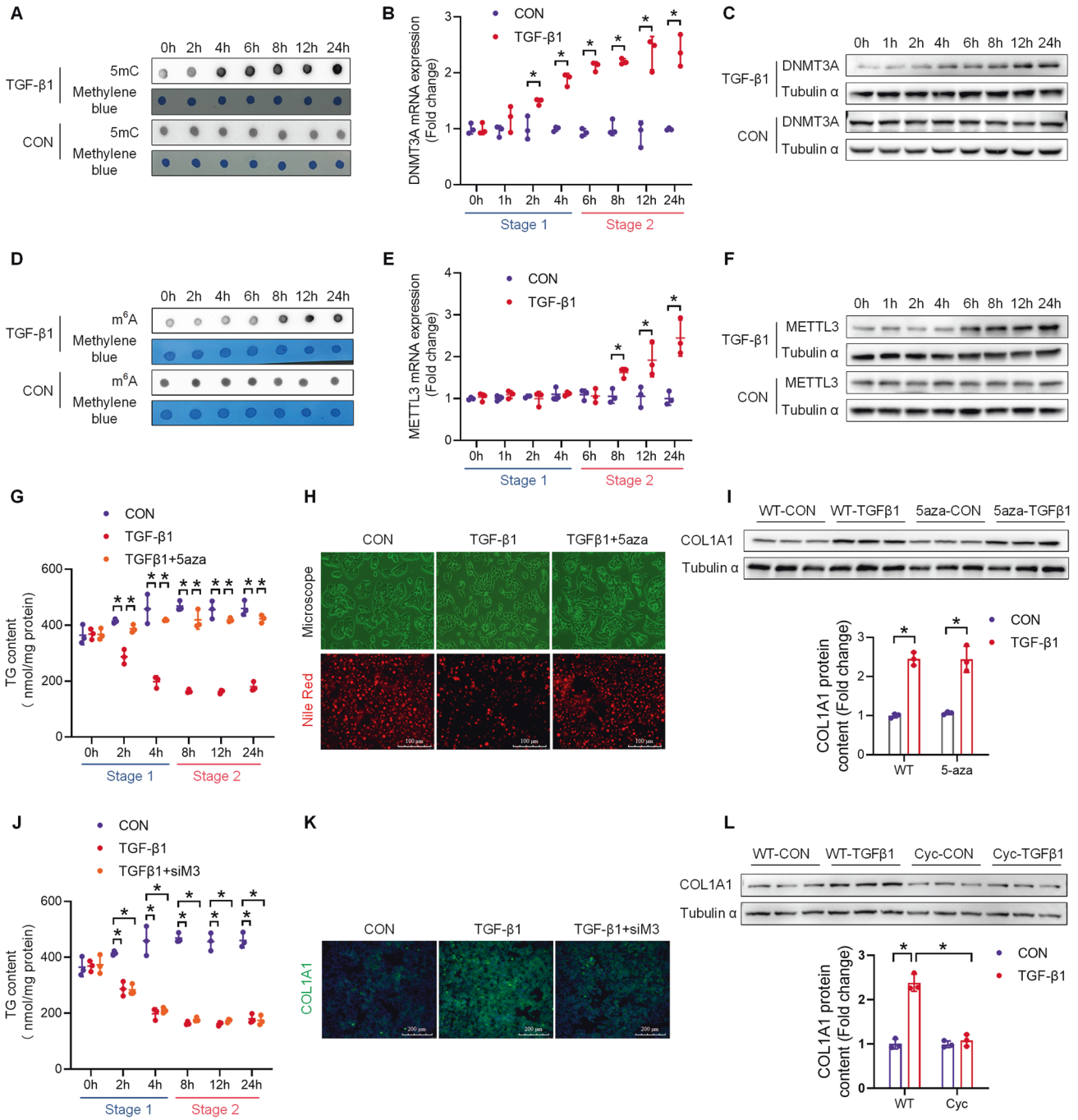

Fig. 2 5mC/m^{6}A modification exhibits stage-specific increase during HSC activation. **A** Total DNA 5mC modification. **B**, **C** mRNA and protein levels of DNMT3A ($n = 3$). **D** Total RNA m^{6}A modification. **E**, **F** mRNA and protein levels of METTL3. **G** Effects of 5mC inhibitor 5-aza treatment on TG content ($n = 3$). **H** Effects of 5-aza treatment on cell morphology and lipid droplet content in the initiation stage. **I** Effects of 5-aza treatment on COL1A1 protein content in the perpetuation stage ($n = 3$). **J** Effects of METTL3 siRNA on TG content ($n = 3$). **K**, **L** METTL3 siRNA and m^{6}A inhibitor cycloleucine on COL1A1 expression in the perpetuation stage ($n = 3$). Stage 1, initiation stage (0–4 h); Stage 2, perpetuation stage (6–24 h). Values are means ± SD, *$p < 0.05$.

COL1A1 production and α-SMA expression in Stage 2 was prohibited (Fig. S1I, J). However, 5-aza administered after HSC-MFB transdifferentiation at 6 h failed to alleviate the increase of COL1A1 expression in Stage 2 (Figs. 2I and S1K). These findings indicate that 5mC specifically regulates the initiation stage of HSC activation.

To elucidate the function of m^{6}A on HSC activation, cells were treated with METTL3 siRNA (siM3, Fig. S1L) or specific m^{6}A inhibitor cycloleucine (cyc), in different stages of activation. siM3 or cyc administered 12 h prior to TGF-β1 stimulation was not able to block the HSC-MFB transdifferentiation in Stage 1 (Figs. 2J and S1M) but significantly inhibited COL1A1 production in Stage 2 (Fig. S1N). Furthermore, siM3 administered after HSC-MFB transdifferentiation at 6 h significantly alleviated the increase of COL1A1 expression in Stage 2 (Figs. 2K and S1O). The same phenomena were observed using m^{6}A inhibitor cyc (Fig. 2L). These findings indicate that m^{6}A specifically regulates the perpetuation stage of HSC activation.

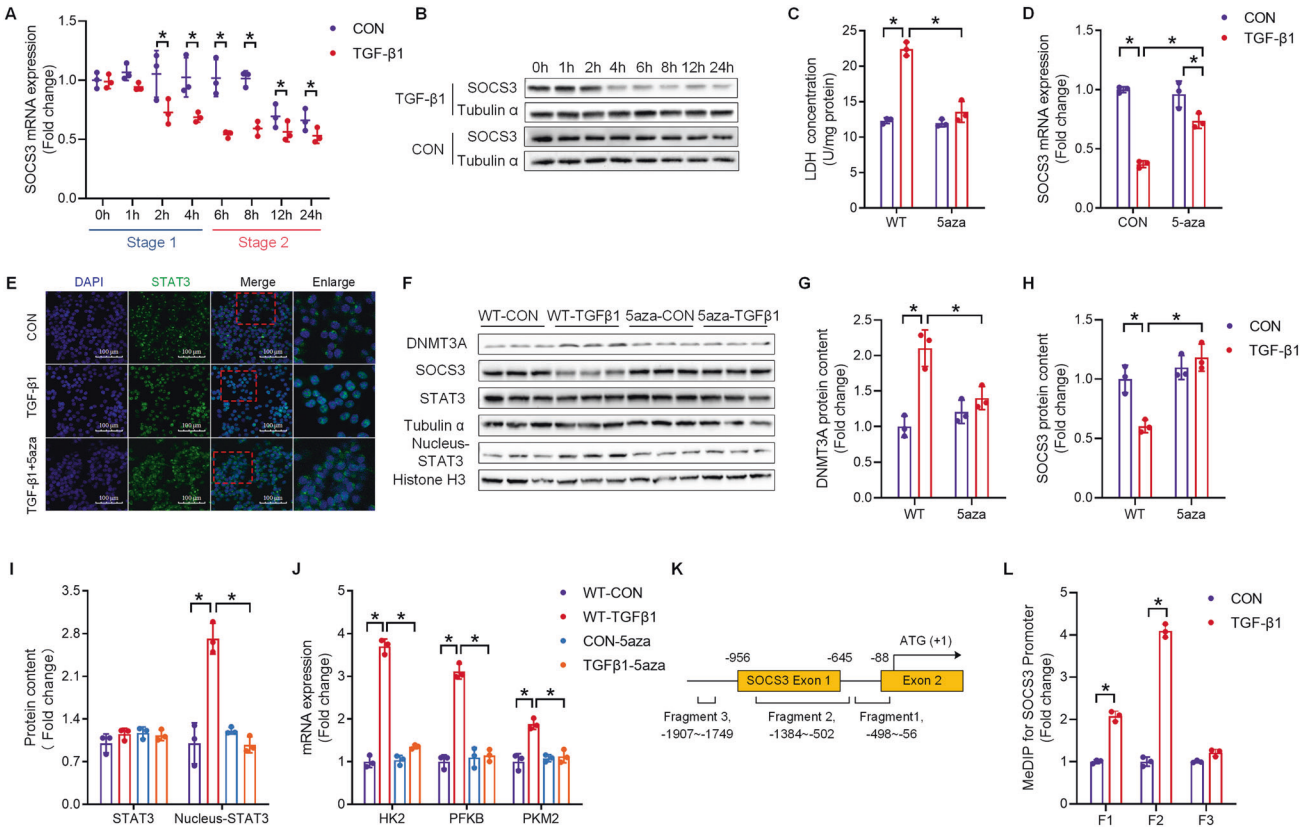

Fig. 3 STAT3 is activated in the initiation stage via 5mC-mediated SOCS3 suppression. A, **B** SOCS3 mRNA and protein levels ($n = 3$). **C** Effects of 5-aza on LDH concentration in the initiation stage ($n = 3$). **D** Effects of 5-aza on SOCS3 mRNA expression at the initiation stage ($n = 3$). **E** Effects of 5-aza on the nuclear translocation of STAT3 at the initiation stage. **F**–**I** Effects of 5-aza on the protein expression of DNMT3A, SOCS3 and STAT3 at the initiation stage ($n = 3$). **J** Effects of 5-aza on the key glycolytic enzymes in the initiation stage ($n = 3$). **K** Schematic diagram of CpG islands on the promoter of SOCS3 gene. **L** 5mC enrichment in SOCS3 gene promoter region at the initiation stage ($n = 3$). Stage 1, initiation stage (0–4 h); Stage 2, perpetuation stage (6–24 h). Values are means ± SD, $^*p < 0.05$.

STAT3 is activated in the initiation stage via 5mC-mediated SOCS3 suppression

JAK-STAT3 pathway is indispensable for metabolic reprogramming of cancer cells via directly or indirectly transactivates the glycolytic enzymes hexokinase 2 (HK2) and pyruvate kinase M2 isoform (PKM2) [29, 30]. Here, the role of STAT3 in metabolic reprogramming during HSC activation was validated by using stattic, a STAT3 inhibitor. Stattic treatment protected HSC from metabolic reprogramming induced by TGF-β1, which is indicated by significantly alleviated activation of glycolytic genes (Fig. S2A) and prohibited an increase of intracellular LDH content (Fig. S2B). The direct action of STAT3 on glycolytic gene transactivation was validated by ChIP-PCR, in which TGF-β1 significantly increased STAT3 binding to predicted binding site on HK2 gene promoter (Fig. S2C–E).

SOCS3 serves as a "brake" in the auto-regulatory feedback loop to prohibit nuclear translocation of STAT3 [31]. Here, a significant downregulation of SOCS3 was detected 2–4 h post TGF-β1 stimulation, at both mRNA (Fig. 3A) and protein (Figs. 3B and S2F) levels, which was associated with metabolic reprogramming in the initiation stage (Fig. S3A–I). The role of SOCS3 in metabolic reprogramming during HSC activation was validated by using SOCS3 overexpression plasmid (pcDNA3.1-SOCS3) transfection (Fig. S2G). SOCS3 overexpression protected HSC from metabolic reprogramming induced by TGF-β1, which is indicated by significantly prohibited an increase of α-SMA expression (Fig. S2G, H) and alleviated activation of glycolytic genes (Fig. S2I). PPARγ is a key transcriptional factor for lipogenesis in HSC [32]. PPARγ downregulation contributes to loss of lipid droplets in Stage 1 of HSC activation. In this study, PPARγ started to decrease 2 h post TGF-β1 treatment and remained low thereafter during HSC activation (Fig. S4A).

5-aza administration 12 h prior to TGF-β1 stimulation partly yet significantly alleviated SOCS3 downregulation at both mRNA (Fig. 3D) and protein (Fig. 3F, H) levels in Stage 1, which was associated with prohibited STAT3 nuclear translocation (Fig. 3E, F, I). Consequently, the activation of rate-limiting glycolytic enzymes (Fig. 3J) was protected by 5-aza, with unaltered intracellular LDH content (Fig. 3C). Similarly, the downregulation of PPARγ in Stage 1 was also prohibited by 5-aza treatment (Fig. S4B). Locus-specific 5mC mapping revealed significant hypermethylation on predicted CpG islands of both SOCS3 and PPARγ gene promoters in activated HSC in Stage 1 (Figs. 3K, L and S4C). Such 5mC-mediated regulation appears to be gene-specific, as TGF-β1 treatment did not affect the 5mC enrichment on glycolytic PFKB and HK2 gene promoters (Fig. S5A–C).

YTHDF1-mediated m^{6}A mechanism contributes to excessive collagen production

Data mining for m^{6}A-modified targets was performed using published m^{6}A-seq databases, focusing on ECM-related transcripts [7, 27]. Many members of the collagen family are reported to have m^{6}A peaks, and mRNA of COL1A1, COL1A2, COL3A1, COL5A2, and COL6A2 was significantly hypermethylated during the perpetuation stage of HSC activation (Figs. 4A and S6A–F). METTL3 siRNA reversed or reduced m^{6}A hypermethylation on collagen mRNAs associated with Stage 2 of HSC activation (Figs. 4A and S6A–F).

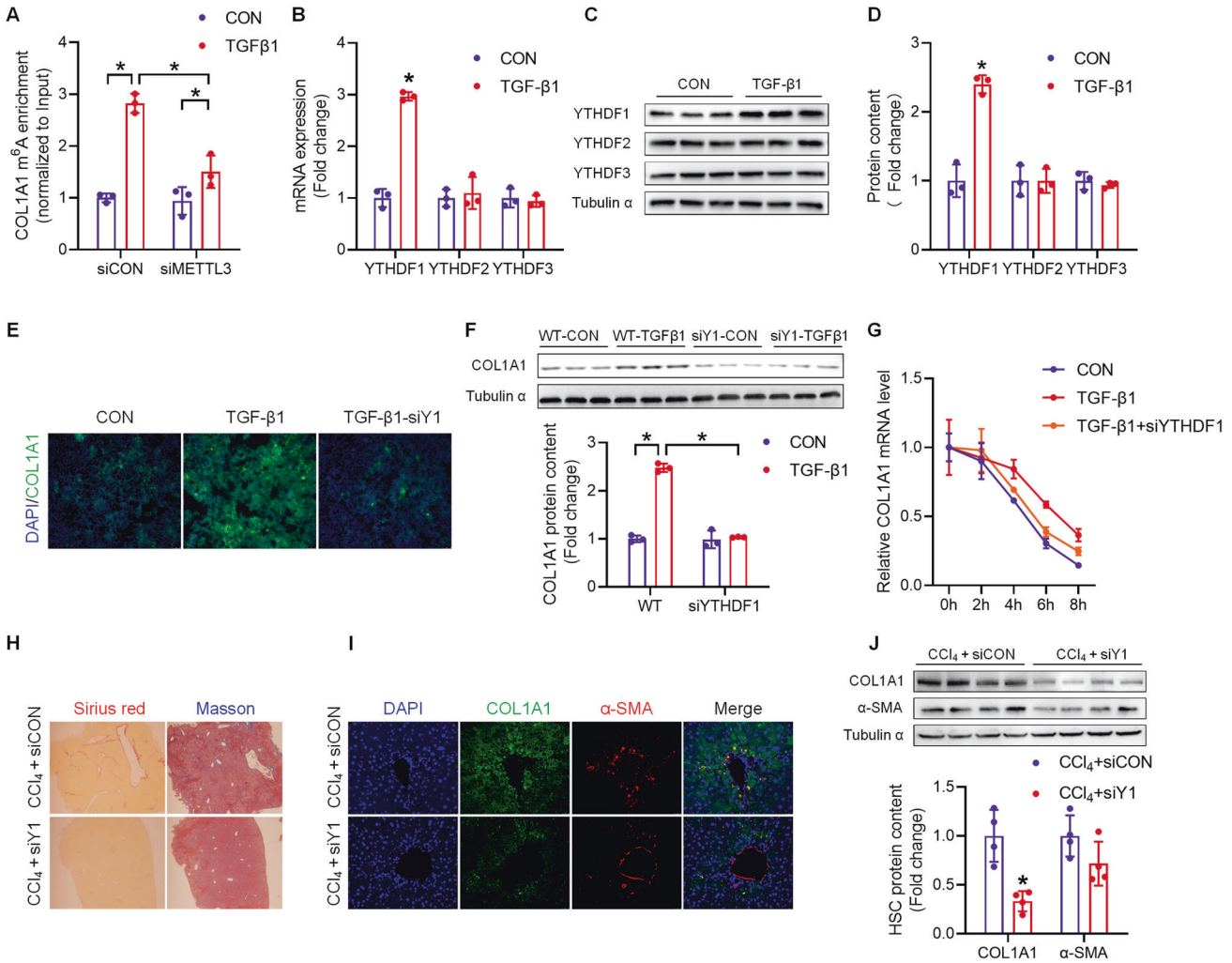

Fig. 4 YTHDF1-mediated m^{6}A mechanism contributes to excessive collagen production. A m^{6}A modification of COL1A1 mRNA in the perpetuation stage and the effect of METTL3 siRNA ($n = 3$). **B–D** YTHDF1, 2 and 3 protein and mRNA expression in the perpetuation stage ($n = 3$). **E, F** Effect of YTHDF1 siRNA on COL1A1 protein content ($n = 3$). **G** Locus-specific m^{6}A modification on COL1A1 mRNAs in the perpetuation stage and the effect of YTHDF1 siRNA ($n = 3$). **H, I** Effect of vitamin A-coupled YTHDF1 siRNA on CCl_4-induced hepatic overproduction of collagens and α-SMA in mice as examined with Sirius red, Masson, and dual-immunofluorescence staining ($n = 4$). **J** COL1A1 and α-SMA protein content in isolated HSC from the liver of vitamin A-coupled siRNA-injected mice ($n = 4$). Values are means ± SD, *$p < 0.05$.

The specific m^{6}A sites in collagen mRNAs were predicted using the SRAMP website (http://www.cuilab.cn/sramp), and the very high confidence m^{6}A modification sites (X site) were verified with the single-base elongation- and ligation-based qPCR amplification method (SELECT) in comparison with the negative control site (N site). m^{6}A on mRNA of all the 5 collagen genes detected was significantly increased in the perpetuation stage of HSC activation (S7A-S7O).

To explore the mechanism by which m^{6}A regulates collagens expression, the expression of m^{6}A reader proteins YTHDF1, 2, and 3 were detected during the perpetuation stage of HSC activation. Among 3 reader proteins, only YTHDF1 was significantly increased (Fig. 4B–D). YTHDF1 knockdown completely prohibited excessive COL1A1 production (Fig. 4E, F). YTHDF1 is reported to act through the m^{6}A-mediated increase in mRNA stability in Hela cells [33]. Here, the mRNA decay analysis using transcription inhibitor actinomycin D indicates an increased half-life of collagen mRNAs in activated HSC. YTHDF1 knockdown significantly decreased the stability of collagen mRNAs (Figs. 4G and S8A–D).

To verify the role of YTHDF1 in hepatic fibrosis in vivo, vitamin A-coupled YTHDF1 siRNA (siY1) was injected into CCl_4-induced liver fibrosis mice (Fig. S9A). Vitamin A-coupled YTHDF1 siRNA treatment significantly attenuated CCl_4-induced weight loss (Fig. S9D) and hepatic collagens overproduction in mice (Figs. 4H and S9B, C). Dual-immunofluorescence staining and western blot show a more pronounced reduction in COL1A1 compared to α-SMA in HSC isolated from siY1-injected mice (Fig. 4I, J), indicating stage-specificity of YTHDF1-mediated hepatic fibrosis alleviation. Hepatocytes, Kupffer cells, and HSC (Fig. S9E–G) isolated from liver samples were used to validate HSC-specific YTHDF1 knockdown (Fig. S9H, I).

HIF-1α links the initiation and the perpetuation stages through transactivating YTHDF1

Time course mapping throughout the entire process of HSC activation revealed a similar pattern of HIF-1α and YTHDF1 expression, which keeps increasing during the perpetuation stage (Figs. 5A–C and S7P, Q). Reciprocal effects between YTHDF1 and HIF-1α using siRNAs indicate that HIF-1α acts as an upstream regulator for YTHDF1, as YTHDF1 knockdown did not affect HIF-1α activation (Fig. 5D, E), whereas HIF-1α knockdown significantly suppressed the transcriptional activation of YTHDF1 (Fig. 5F, G).

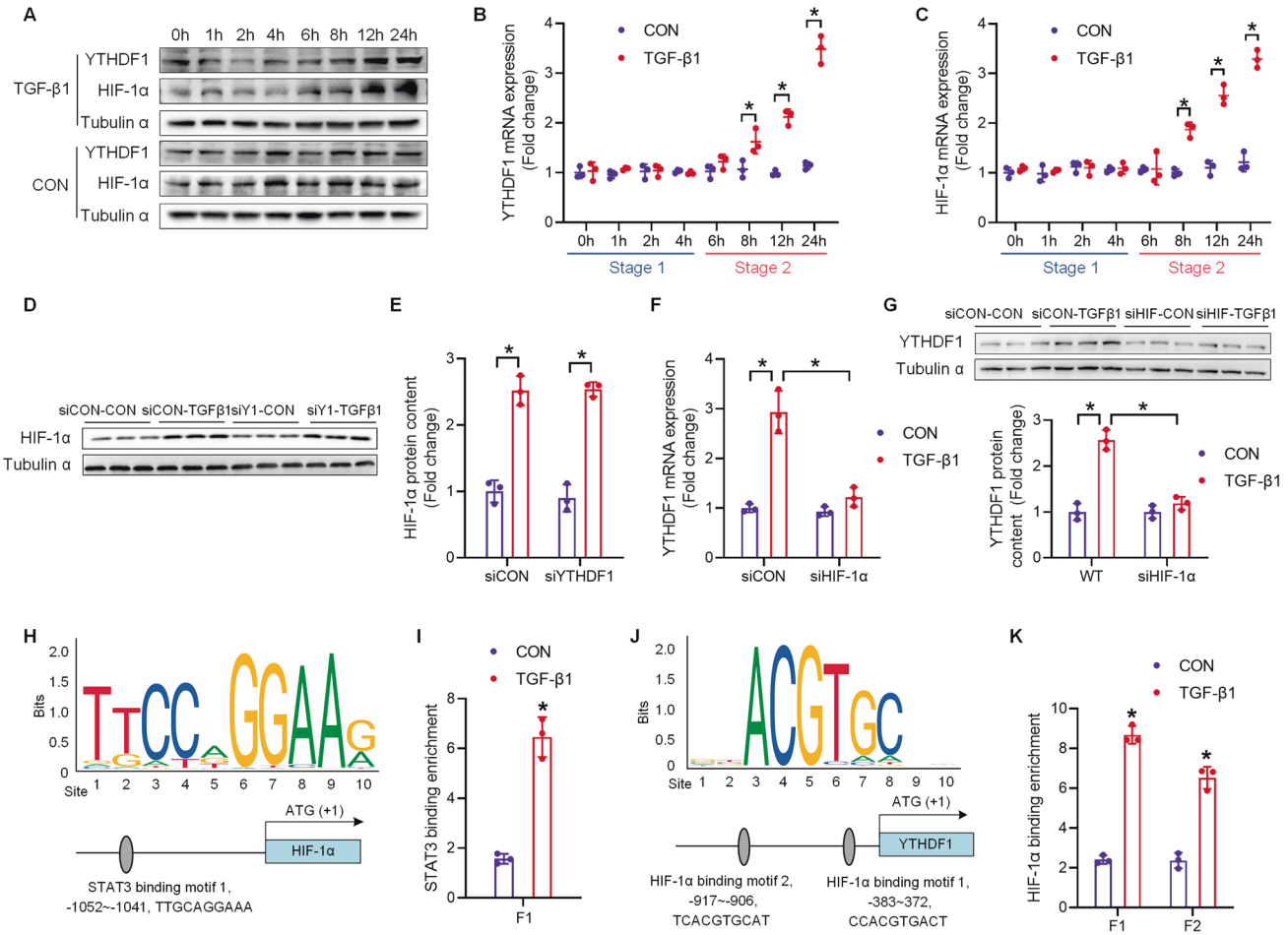

Fig. 5 HIF-1α links the initiation and the perpetuation stages through transactivating YTHDF1. A–**C** YTHDF1 and HIF-1α mRNA and protein levels ($n = 3$). **D**, **E** Effect of YTHDF1 siRNA on HIF-1α protein content in the perpetuation stage ($n = 3$). **F**, **G** Effect of HIF-1α siRNA on YTHDF1 protein content in the perpetuation stage ($n = 3$). **H**, **I** Schematic diagram of STAT3 binding site on the promoter region of HIF-1α gene and the abundance of STAT3 binding in the initiation stage ($n = 3$). **J**, **K** Schematic diagram of HIF-1α binding site on the promoter region of YTHDF1 gene and the abundance of HIF-1α binding in the perpetuation stage ($n = 3$). Values are means ± SD, *$p < 0.05$.

A HIF-1α binding site was predicted in the promoter region of YTHDF1 gene and the binding of HIF-1α to YTHDF1 gene promoter was significantly increased in activated HSC in Stage 2 (Fig. 5J, K). Moreover, STAT3 binding to its predicted sites on HIF-1α gene promoter was also significantly increased during HSC activation in Stage 1 (Fig. 5H, I). These results suggest a cascade of gene transactivation during HSC activation. Activated STAT3 in the initiation stage transactivates HIF-1α. HIF-1α then transactivates YTHDF1 and thereby increasing collagen mRNA stability and collagen overproduction in m^{6}A-dependent manner.

DISCUSSION

Epigenetic dysregulation of gene expression is the core to the pathophysiology of metabolic-associated diseases. All means of epigenetic mechanisms, including RNA and DNA methylation, histone modifications, and non-coding RNAs, are reported to participate in NAFLD progression [34]. Nevertheless, it has been a great challenge to delineate the complex interplay among different means of epigenetic regulation in multifactorial diseases [35]. Here, we show that DNA 5mC and RNA m^{6}A modification successively facilitates the initiation and perpetuation stages of HSC activation in hepatic fibrosis progression. Our findings clarify the previous controversy over the alterations and the roles of these epigenetic marks in hepatic fibrosis progression. DNA 5mC and RNA m^{6}A marks are highly dynamic in different cell types. Studies in vivo using liver samples are complexed by mixed cell types and diverse stages of disease progression, while studies in vitro using primary HSC or cell lines may come up with ambiguous results due to the heterogeneity of activation stages. In this study, we distinguished the initiation and perpetuation stages of HSC activation in vitro and characterized the dynamic changes and collaborative functions of 5mC/m^{6}A methylation (Fig. 6).

It is intriguing that DNA 5mC modification specifically regulates the initiation stage of HSC activation which is associated with metabolic reprogramming. The role of 5mC modification in metabolic reprogramming has been reported in various cancer cells [36, 37]. It appears that genes coding for glycolytic enzymes are direct targets for 5mC-mediated gene activation in cancerous cells. For instance, hypomethylation of HK2 gene promoter directly leads to its activation in hepatocellular carcinoma and glioblastoma [38, 39]. During the initiation stage of HSC activation, however, no alterations are detected for DNA 5mC modification on the promoter of HK2 or PFKB genes. Therefore, glycolytic enzymes may not be the direct targets for DNA 5mC-mediated gene regulation during metabolic reprogramming of HSC. SOCS3 acts as a negative regulator of JAK/STAT3 pathway via an auto-regulatory feedback loop [31]. Reduced expression of SOCS3 leads to unrestricted activation of the JAK2-STAT3 signaling pathway and subsequent metabolic reprogramming in cancerous cells [31, 40]. A similar mechanism applies in metabolic reprogramming

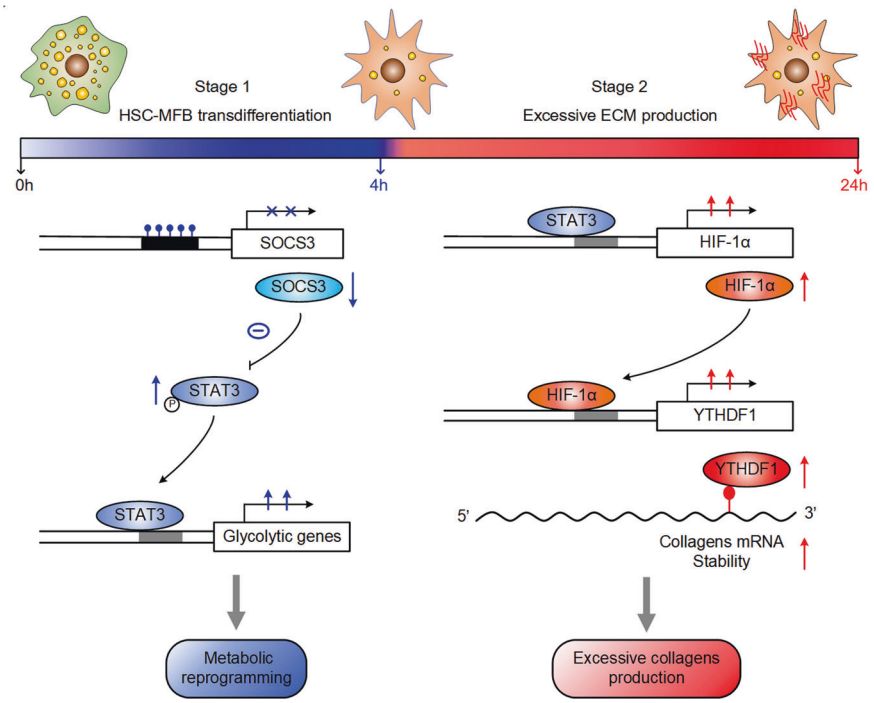

Fig. 6 Proposed working model of the proposed mechanism in this study. A time-course mapping throughout the process of TGF-β1-induced HSC activation to differentiate the initiation and perpetuation stages. DNA 5mC hypermethylation on the promoter of SOCS3 gene leads to metabolic reprogramming in the initiation stage, and m6A hypermethylation on transcripts of collagen family exacerbates collagen production in a YTHDF1-dependent manner during the perpetuation stage. STAT3-activated HIF-1α pathway serves as a bridge linking the initiation stage and the perpetuation stage in HSC activation.

during the initiation stage of HSC activation. Significant DNA 5mC hypermethylation occurs in the promoter region of SOCS3 gene, leading to its transcriptional repression in HSC cells. This is inconsistent with skin fibroblasts activation, in which 5mC modification in the SOCS3 promoter region is significantly elevated, thereby leading to its repression and overactivation of the JAK2-STAT3 pathway [41].

Loss of lipid droplets is another mark for HSC-MFB transdifferentiation during the initiation stage of HSC activation. The lipogenic gene PPARγ is also subjected to 5mC hypermethylation on the promoter region, which results in decreased PPARγ expression and impaired lipogenesis in HSC. Similar 5mC-based epigenetic regulation on PPARγ has been reported in mouse pulmonary fibrosis and lung fibroblast activation [42]. Obviously, SOCS3 and PPARγ are unlikely the only target genes for 5mC modification during the initiation stage of HSC activation, as the methyltransferase DNMT3A is significantly upregulated in the initiation stage. A high-throughput analysis is required to constitute the network of genes subjected to DNA 5mC-mediated regulation, using MeDIP-seq and/or DNMT3A-anchored ChIP-seq approaches. Smad3, which is activated by TGF-β1, is reported to transactivate DNMT3A during skin fibroblast activation [41]. A similar signaling pathway is speculated to be responsible for DNMT3A upregulation and 5mC hypermethylation in TGF-β1-activated HSC during the initiation stage.

It has been reported that DNA 5mC hypermethylation is associated with the progression of liver fibrosis in vivo [43]. The human fibrotic liver displays a global hyper-5mC modification and upregulation of DNMT3A/B [6]. Moreover, DNA hypermethylation on PPARγ gene promoter in human liver biopsy samples [44] or cell-free DNA of human plasma [45] is suggested to serve as a potential biomarker for the severity of liver fibrosis. These results correlate with the overall hypermethylation in primary HSC isolated from mice with CCl_4-induced liver fibrosis [46]. Also, the DNMTs inhibitor 5-aza blocks transdifferentiation of rat primary HSC, thus preventing the acquisition of proinflammatory and profibrogenic traits [16]. Mechanistically, DNA hypermethylation in the promoter regions of antifibrogenic PPARγ and IκBα genes promotes liver fibrosis progression [16]. In this study, using the murine SV40 immortalized HSC line JS1, we pinpointed that DNA hypermethylation on the promoter regions of SOCS3 and PPARγ genes regulates specifically the initiation stage, and does not participate in the perpetuation stage of HSC activation.

Previous studies on the role of RNA m^6A modification in NAFLD progression have produced paradoxical results. This is also caused by mixed cell types and diverse stages of NAFLD progression. During a simple fatty liver and hepatocyte lipid deposition, global m^6A modification is significantly reduced, which inhibits YTHDF2-mediated degradation of lipogenic mRNAs (SREBP1, FASN, and SCD) and leads to excessive lipid deposition in hepatocytes [47]. During steatohepatitis and KC activation, global m^6A modification is significantly increased, together with significant hypermethylation on the 5'UTR of TGF-β1 mRNA, which promotes cap-independent TGF-β1 translation and accelerates hepatitis to fibrosis transformation [5]. Both decrease and increase of m^6A modifications are reported in the CCl_4-induced mouse model of liver fibrosis [7, 18]. The disparity may attribute to differences in samples (whole liver vs. primary HSC) and stages of fibrosis progression. Recent studies have sought to clarify the relationship between hyper-m^6A modification and liver fibrosis, and the mechanisms underlying the role of m^6A in liver fibrosis vary in the different studies using different models. In CCl_4-activated primary HSC, METTL3 is significantly increased, which inhibits Hedgehog pathway activation and enhances fibrosis-related gene expression via m^6A-YTHDF2-dependent silencing of GPR161 mRNA [48]. HSC-specific knockout of METTL3 reduces m^6A deposition on Lats2 mRNA, thereby increasing their stability. Elevated Lats2 increases phosphorylation of the downstream transcription factor YAP, thus suppressing YAP nuclear translocation, which ultimately suppresses HSC activation and significantly

alleviates CCl_4-induced liver fibrosis [49]. Studies in vivo using liver samples are complexed by mixed cell types and diverse stages of disease progression, while studies in vitro using primary HSC or cell lines harvested at a single time point may come up with ambiguous results due to the heterogeneity of activation stages. In this study, we performed a time-course analysis using HSC cell line JS1 to distinguish the initiation and perpetuation stages of HSC activation and characterized the dynamic changes and collaborative functions of 5mC/m^6A methylation. We found that hyper-m^6A modification is associated with HSC activation and pinpointed the specific role of m^6A modification in the perpetuation stage of HSC activation, by directly targeting on major collagen genes.

The signaling pathway that governs the "relay" of 5mC and m^6A modification in regulating HSC activation cascade is of great interest. In this study, we demonstrate that 5mC-mediated SOCS3 suppression leads to STAT3 activation. STAT3 transactivates HIF-1α and HIF-1α subsequentially transactivates YTHDF1, thus linking 5mC- mediated initiation stage and m^6A-dependent perpetuation stage of HSC activation cascade. As most of the m^6A-related genes, such as METTL3 [50], METTL14 [51], and ALKBH5 [52], have CpG islands on their promoter regions, they can be the direct targets for 5mC- mediated regulation. In pancreatic cancer, cigarette smoke condensate (CSC) induces hypomethylation of METTL3 gene promoter, which leads to the upregulation of METTL3 [50]. Moreover, CSC leads to hypomethylation of CpG island on ALKBH5 gene promoter, thus resulting in diminished m^6A abundance in esophageal squamous cell carcinoma [52]. Nevertheless, the direct link between DNA 5mC and RNA m^6A modification is unlikely in HSC activation cascade, as 5-aza treatment in the perpetuation stage has no effect on either m^6A-metabolic enzymes or collagen production. Our results indicate that intervention of DNA 5mC modification blocks the initiation stage and certainly the subsequent perpetuation stage of HSC activation, while the intervention of RNA m^6A modification only alleviates the perpetuation stage of HSC activation. Considering the heterogeneity and the vicious cycle of HSC activation in hepatic fibrosis progression in vivo, the combined intervention of 5mC/m^6A may benefit the prognosis of hepatic fibrosis.

In summary, we demonstrate, for the first time, successive and synergistic roles of DNA 5mC and RNA m^6A modification in the cascade of HSC activation. Moreover, the specific targets of 5mC- and m^6A-mediated epigenetic regulation are identified and the molecular links between 5mC- and m^6A-mediated machineries are clarified. These findings provide novel insights into the molecular mechanisms underlying HSC activation and implicate new therapeutic strategies for treating liver fibrosis and cirrhosis.

METHODS

Cell culture and treatment

JS1, a murine SV40 immortalized HSC line with a highly activated phenotype [21], was purchased from BeNa Biology Institute (BNCC359737). JS1 cells were cultured in DMEM (319-005, Wisent, China) containing 10% fetal bovine serum (10099141, Gibco, USA) and 1% penicillin/streptomycin (15070063, Gibco, USA) at 37°C under 5% CO_2. Cells were cultured to 80% confluence and then treated with 10 ng/ml TGF-β1 (HY-P7117, MedChemExpress, USA) for 12 h.

Mice and treatment

Sixteen C57BL/6 mice (6-week-old, male) were purchased from Model Animal Research Center of Nanjing University (Nanjing, China). Following 1 week of adaptive feeding, the mice were randomly divided into CCl_4 + siCON and CCl_4 + siYTHDF1 groups. Both groups were injected intraperitoneally with 5 ml/kg of 10% carbon tetrachloride (CCl_4) twice a week for 4 weeks, to establish liver fibrosis. The day before each CCl_4 injection, mice from CCl_4 + siCON group were injected through the tail vein with vitamin A-coupled scrambled siRNA and those from CCl_4 + siYTHDF1 group injected with vitamin A-coupled YTHDF1 siRNA (Fig. S9A). At the end of experiment, mice were euthanized and the primary HC [22], KC [22] and HSC [23] were isolated from the liver according to previous publications.

Preparation of vitamin A-coupled siRNA

Vitamin A-coupled siRNA was prepared as described previously with slight modification [24]. Instead of using vitamin A-coupled liposomes to carry siRNA, we used chemically modified YTHDF1 siRNA (5′-GGAAAUGCCCAAC CUACTT-3′) or scrambled siRNA (5′-UUCUCCGAACGUGUCACGUTT-3′) with 5′-Chol and 2′-OMe to increase the bioavailability and stability (RiboBio, China). Each mouse was received a bolus injection of a freshly prepared mixture (10 nmol siRNA and 200 μmol vitamin A dissolved in 200 μl saline and rotated at 37 °C for 30 min) each time.

Immunofluorescence staining

Intracellular localization of COL1A1 (BA0325, Boster Biological Technology, China, diluted 1:100) and STAT3 (ab68153, Abcam, USA, diluted 1:500) was visualized by immunofluorescence staining with Alexa Fluor® 488 conjugated donkey anti-rabbit IgG (ab150073, Abcam, USA, diluted 1:1000). Cell nuclei were stained with 4,6-diamidino-2-phenylindole (DAPI, Molecular probes, diluted 1:1000) and the lipid droplets were labeled with Nile red (N1142, Invitrogen, USA, diluted 1:10,000). Immunofluorescent images were captured with a confocal laser scanning microscope (×40 magnification) with Z-scan analysis (Olympus IX 81, Olympus, Japan).

RNA isolation, real-time quantitative PCR (qPCR)

Total RNA was isolated by using TRIzol Reagent (TSP401, Tsingke Biotech, China), and 1 μg of RNA was reverse-transcribed into cDNA by using a HiScript® II Reverse Transcriptase kit (R233-01, Vazyme, China) according to the manufacturer's protocol. In total, 2 μl of diluted cDNA (1:20, v-v) was used for real-time quantitative PCR by using a QuantStudio™ 6 Flex Real-Time PCR System, 384-well (Thermo Scientific, USA). All primers (Supplementary Table 1) were synthesized by Tsingke Biotech (Nanjing, China). PPIA, which was not affected by the treatment, was chosen as a reference gene. Data were analyzed by using the method of $2^{-\Delta\Delta CT}$.

Protein extraction and Western blot analysis

The protein concentration of the cell lysates was measured by the BCA Protein Assay kit (DQ111-01, TransGen Biotech, China). In total, 20 μg proteins were used for electrophoresis on a 10 or 15% SDS-PAGE gel and transferred onto a nitrocellulose membrane. The primary antibodies used for Western blot analysis were listed in Supplementary Table 2. Tubulin α was selected as an internal control. Images were captured by VersaDoc 4000MP system (Bio-Rad, USA), and the band density was analyzed with Quantity One software (Bio-Rad, USA).

DNA 5mC and RNA m^6A dot blot assay

DNA samples were diluted to 250 ng/μl and heated at 95 °C for 10 min to denature DNA. Samples were immediately placed on ice for 5 min, and 1 μl was loaded per dot on Hybond-N^+ membranes (GE Healthcare). The DNA was crosslinked in a UV Stratalinker, blocked for 1 h in 5% non-fat milk, and probed overnight at 4 °C with an anti-5mC antibody (AB10805, Abcam, diluted 1:1000). The membrane was washed three times for 10 min with TBST and then probed with a secondary antibody in 5% milk for 2 h at room temperature. For m^6A dot blotting, 500 ng RNA sample was denatured at 95 °C for 5 min and transferred onto a Hybond-N^+ membrane. After UV cross-linking, the membrane was washed with TBST buffer, blocked with 5% non-fat milk, and incubated with an anti-m^6A antibody (AB151230, Abcam, diluted 1:1000) overnight at 4 °C. Then, the membrane was incubated with a secondary antibody at room temperature for 2 h. The signals were visualized by a chemiluminescence system (Bio-Rad, USA), and the dot density was analyzed with Quantity One software (Bio-Rad, USA). Before blocking, the DNA and RNA dot blots were stained with 0.02% methylene blue (in 0.3 mol/l sodium acetate, pH = 5.2) as loading controls.

Methylated DNA immunoprecipitation (MeDIP) assay

Methylated DNA immunoprecipitation (MeDIP) analysis was performed as previously described with some modifications [25]. Purified genomic DNA from JS1 cells was fragmented to a mean size of 300 base pairs (bp), and

1 μg of fragmented DNA was heat-denatured and immunoprecipitated with a 5-mC antibody (AB10805, Abcam, USA). The precipitated immune complexes were captured by pretreated protein G agarose beads (40 μl, 50% slurry, sc-2003, Santa Cruz Biotechnology, USA), and purified MeDIP DNA was used to amplify the proximal promoter sequences of the target genes by real-time PCR (Supplementary Table 3). CpG islands of the proximal promoters were predicted with Methprimer [26].

Chromatin immunoprecipitation (ChIP) assay

Cells were crosslinked in 1% formaldehyde and quenched by addition of 125 mM glycine, scraped, and collected by centrifugation, then washed twice with cold phosphate-buffered saline. Cells from 10 cm plate were lysed with 1 ml sodium dodecyl sulfate lysis buffer containing protease inhibitor cocktail (11697498001; Roche, USA). Crude chromatin preparations were sonicated on ice to yield DNA fragments of 150–300 bp in length and precleared with salmon sperm DNA-treated protein A/G agarose beads (40 μl, 50% slurry, sc-2003, Santa Cruz Biotechnology, USA). The precleared chromatin preparations were incubated with 2 μg primary antibody against STAT3 (AB68153, Abcam, USA) overnight at 4 °C. A negative control was included with normal IgG (2729S, Cell Signaling Technology, USA). Protein A/G agarose beads were added to capture the immunoprecipitated chromatin complexes. Finally, DNA fragments were released from the immunoprecipitated complexes by reverse cross-linking at 65 °C for 1 h, and quantitative real-time PCR was used to quantify the fragments of target gene promoters with specific primers (Supplementary Table 3).

Methylated RNA immunoprecipitation (MeRIP) assay

Total RNA was isolated and chemically fragmented at 94 °C for 5 min in a fragmentation buffer (0.1 M $ZnCl_2$, 0.1 M Tris-HCl, pH = 7.0) to ~150–300 bp in size, ethanol-precipitated and purified using an EasyPure RNA Purification Kit (ER701-01; TransGen, China). In total, 40 μg fragmented total RNA was precleared with protein A/G agarose beads (40 μl, sc-2003, Santa Cruz Biotechnology, USA) supplemented with 40U RNase inhibitor overnight at 4 °C. The mixture was incubated with 2 μg m^6A antibody (ab151230, Abcam, USA) overnight at 4 °C. A negative control was included with normal IgG (2729S, Cell Signaling Technology, USA). Protein A/G agarose beads were added to capture the immunoprecipitated complexes. RNA was eluted from the beads with 300 μl of elution buffer (5 mM Tris-HCl, 1 mM EDTA and 0.05% sodium dodecyl sulfate) with 20 μg of proteinase K for 1 h at 60 °C. Following phenol extraction and ethanol precipitation, the input and m^6A enriched RNA were reversely transcribed with random hexamers, and the m^6A enrichment on specific transcripts was determined by qPCR. The primers used for detecting m^6A-enriched mRNAs were shown in Supplementary Table 4.

SELECT for the detection of m^6A

From previously published m^6A-seq databases [7, 27], sequences with m^6A peaks were retrieved for collagen mRNAs and subjected to specific m^6A site prediction with SRAMP (http://www.cuilab.cn/sramp). One very high/high confidence m^6A site was selected for each mRNA and verified using a single-base elongation- and ligation-based qPCR amplification method (termed "SELECT") [28]. The SELECT products of indicated sites were normalized to the abundance of respective RNAs (inputs). Primers used in the SELECT assay are listed in Supplementary Table 5.

siRNA transfection and inhibitor treatment

JS1 cells at 60% confluence were transfected with siRNAs specifically designed and verified to knockdown the expression of METTL3 (siB171201025317, RiboBio, China), YTHDF1 (siG151229103951, RiboBio, China), and HIF-1α (siB11426115323, RiboBio, China). Cells were seeded onto a 6-well plate for transfection using Lipofectamine 2000 (Invitrogen, USA), following the manufacturer's instructions.

RNA decay assay

JS1 cells were cultured in 6-well plates followed by the treatment with or without TGF-β1 or YTHDF1 siRNA. Then actinomycin D (HY-17559, MCE, USA) was added to each well to a final concentration of 5 μg/ml to inhibit de novo transcription. Cells were collected at 0, 2, 4, 6, and 8 h after the administration of actinomycin D. Total RNA was isolated and subjected to RT-qPCR to quantify the relative abundance of collagen mRNAs (relative to 0 h).

Statistical analysis

All data are presented as mean ± SD. All experiments were repeated at least twice. The differences between groups were analyzed using Student's *t* test or two-way analysis of variance followed by Tukey's test for multiple comparisons with SPSS 20.0 (IBM, Armonk, NY). The differences were considered statistically significant when $p < 0.05$.

DATA AVAILABILITY

Data supporting the present study are available from the corresponding author upon reasonable request.

REFERENCES

1. Younossi ZM, Blissett D, Blissett R, Henry L, Stepanova M, Younossi Y, et al. The economic and clinical burden of nonalcoholic fatty liver disease in the United States and Europe. Hepatology. 2016;64:1577–86.
2. Kumar R, Priyadarshi RN, Anand U. Non-alcoholic fatty liver disease: growing burden, adverse outcomes and associations. J Clin Transl Hepatol. 2020;8:76–86.
3. Hu Y, Feng Y, Zhang L, Jia Y, Cai D, Qian SB, et al. GR-mediated FTO transactivation induces lipid accumulation in hepatocytes via demethylation of m(6)A on lipogenic mRNAs. RNA Biol. 2020;17:930–42.
4. Hyun J, Jung Y. DNA methylation in nonalcoholic fatty liver disease. Int J Mol Sci. 2020;21:8138.
5. Feng Y, Dong H, Sun B, Hu Y, Yang Y, Jia Y, et al. METTL3/METTL14 transactivation and m(6)A-dependent TGF-β1 translation in activated Kupffer cells. Cell Mol Gastroenterol Hepatol. 2021;12:839–56.
6. Page A, Paoli P, Moran Salvador E, White S, French J, Mann J. Hepatic stellate cell transdifferentiation involves genome-wide remodeling of the DNA methylation landscape. J Hepatol. 2016;64:661–73.
7. Fan C, Ma Y, Chen S, Zhou Q, Jiang H, Zhang J, et al. Comprehensive analysis of the transcriptome-wide m6A methylation modification difference in liver fibrosis mice by high-throughput m6A sequencing. Front Cell Dev Biol. 2021;9:767051.
8. Cancer Genome Atlas Research Network. Comprehensive and integrative genomic characterization of hepatocellular carcinoma. Cell. 2017;169:1327–41.e23.
9. Chen M, Wei L, Law CT, Tsang FH, Shen J, Cheng CL, et al. RNA N6-methyladenosine methyltransferase-like 3 promotes liver cancer progression through YTHDF2-dependent posttranscriptional silencing of SOCS2. Hepatology. 2018;67:2254–70.
10. Ma JZ, Yang F, Zhou CC, Liu F, Yuan JH, Wang F, et al. METTL14 suppresses the metastatic potential of hepatocellular carcinoma by modulating N(6)-methyladenosine-dependent primary MicroRNA processing. Hepatology. 2017;65:529–43.
11. Puche JE, Saiman Y, Friedman SL. Hepatic stellate cells and liver fibrosis. Compr Physiol. 2013;3:1473–92.
12. Tsuchida T, Friedman SL. Mechanisms of hepatic stellate cell activation. Nat Rev Gastroenterol Hepatol. 2017;14:397–411.
13. Dewidar B, Meyer C, Dooley S, Meindl-Beinker AN. TGF-β in hepatic stellate cell activation and liver fibrogenesis-updated 2019. Cells. 2019;8:1419.
14. Trivedi P, Wang S, Friedman SL. The power of plasticity-metabolic regulation of hepatic stellate cells. Cell Metab. 2021;33:242–57.
15. Friedman SL, Pinzani M. Hepatic fibrosis 2022: unmet needs and a blueprint for the future. Hepatology. 2022;75:473–88.
16. Mann J, Oakley F, Akiboye F, Elsharkawy A, Thorne AW, Mann DA. Regulation of myofibroblast transdifferentiation by DNA methylation and MeCP2: implications for wound healing and fibrogenesis. Cell Death Differ. 2007;14:275–85.
17. Shi H, Wei J, He C. Where, when, and how: context-dependent functions of RNA methylation writers, readers, and erasers. Mol Cell. 2019;74:640–50.
18. Yang JJ, Wang J, Yang Y, Yang Y, Li J, Lu D, et al. ALKBH5 ameliorated liver fibrosis and suppressed HSCs activation via triggering PTCH1 activation in an m(6)A dependent manner. Eur J Pharmacol. 2022;922:174900.
19. Shen M, Li Y, Wang Y, Shao J, Zhang F, Yin G, et al. N(6)-methyladenosine modification regulates ferroptosis through autophagy signaling pathway in hepatic stellate cells. Redox Biol. 2021;47:102151.
20. Shen M, Guo M, Li Y, Wang Y, Qiu Y, Shao J, et al. m(6)A methylation is required for dihydroartemisinin to alleviate liver fibrosis by inducing ferroptosis in hepatic stellate cells. Free Radic Biol Med. 2022;182:246–59.
21. Ghiassi-Nejad Z, Hernandez-Gea V, Woodrell C, Lang UE, Dumic K, Kwong A, et al. Reduced hepatic stellate cell expression of Kruppel-like factor 6 tumor suppressor isoforms amplifies fibrosis during acute and chronic rodent liver injury. Hepatology. 2013;57:786–96.
22. Aparicio-Vergara M, Tencerova M, Morgantini C, Barreby E, Aouadi M. Isolation of Kupffer cells and hepatocytes from a single mouse liver. Methods Mol Biol. 2017;1639:161–71.

23. Mederacke I, Dapito DH, Affò S, Uchinami H, Schwabe RF. High-yield and high-purity isolation of hepatic stellate cells from normal and fibrotic mouse livers. Nat Protoc. 2015;10:305–15.
24. Sato Y, Murase K, Kato J, Kobune M, Sato T, Kawano Y, et al. Resolution of liver cirrhosis using vitamin A-coupled liposomes to deliver siRNA against a collagen-specific chaperone. Nat Biotechnol. 2008;26:431–42.
25. Cai D, Yuan M, Jia Y, Liu H, Hu Y, Zhao R. Maternal gestational betaine supplementation-mediated suppression of hepatic cyclin D2 and presenilin1 gene in newborn piglets is associated with epigenetic regulation of the STAT3-dependent pathway. J Nutr Biochem. 2015;26:1622–31.
26. Li LC, Dahiya R. MethPrimer: designing primers for methylation PCRs. Bioinformatics. 2002;18:1427–31.
27. Li T, Zhuang Y, Yang W, Xie Y, Shang W, Su S, et al. Silencing of METTL3 attenuates cardiac fibrosis induced by myocardial infarction via inhibiting the activation of cardiac fibroblasts. FASEB J. 2021;35:e21162.
28. Xiao Y, Wang Y, Tang Q, Wei L, Zhang X, Jia G. An elongation- and ligation-based qPCR amplification method for the radiolabeling-free detection of locus-specific N(6)-methyladenosine modification. Angew Chem. 2018;57:15995–16000.
29. Jiang S, Zhang LF, Zhang HW, Hu S, Lu MH, Liang S, et al. A novel miR-155/miR-143 cascade controls glycolysis by regulating hexokinase 2 in breast cancer cells. EMBO J. 2012;31:1985–98.
30. Poli V, Camporeale A. STAT3-mediated metabolic reprograming in cellular transformation and implications for drug resistance. Front Oncol. 2015;5:121.
31. Carow B, Rottenberg ME. SOCS3, a major regulator of infection and inflammation. Front Immunol. 2014;5:58.
32. Lee YK, Park JE, Lee M, Hardwick JP. Hepatic lipid homeostasis by peroxisome proliferator-activated receptor gamma 2. Liver Res. 2018;2:209–15.
33. Wang X, Zhao BS, Roundtree IA, Lu Z, Han D, Ma H, et al. N(6)-methyladenosine modulates messenger RNA translation efficiency. Cell. 2015;161:1388–99.
34. Rodríguez-Sanabria JS, Escutia-Gutiérrez R, Rosas-Campos R, Armendáriz-Borunda JS, Sandoval-Rodríguez A. An update in epigenetics in metabolic-associated fatty liver disease. Front Med. 2021;8:770504.
35. Chen YT, Shen JY, Chen DP, Wu CF, Guo R, Zhang PP, et al. Identification of cross-talk between m(6)A and 5mC regulators associated with onco-immunogenic features and prognosis across 33 cancer types. J Hematol Oncol. 2020;13:22.
36. Kaelin WG Jr, McKnight SL. Influence of metabolism on epigenetics and disease. Cell. 2013;153:56–69.
37. Sun L, Zhang H, Gao P. Metabolic reprogramming and epigenetic modifications on the path to cancer. Protein Cell. 2021;13:877–919.
38. Goel A, Mathupala SP, Pedersen PL. Glucose metabolism in cancer. Evidence that demethylation events play a role in activating type II hexokinase gene expression. J Biol Chem. 2003;278:15333–40.
39. Wolf A, Agnihotri S, Munoz D, Guha A. Developmental profile and regulation of the glycolytic enzyme hexokinase 2 in normal brain and glioblastoma multiforme. Neurobiol Dis. 2011;44:84–91.
40. Huang L, Hu B, Ni J, Wu J, Jiang W, Chen C, et al. Transcriptional repression of SOCS3 mediated by IL-6/STAT3 signaling via DNMT1 promotes pancreatic cancer growth and metastasis. J Exp Clin Cancer Res. 2016;35:27.
41. Dees C, Pötter S, Zhang Y, Bergmann C, Zhou X, Luber M, et al. TGF-β-induced epigenetic deregulation of SOCS3 facilitates STAT3 signaling to promote fibrosis. J Clin Investig. 2020;130:2347–63.
42. Wei A, Gao Q, Chen F, Zhu X, Chen X, Zhang L, et al. Inhibition of DNA methylation de-represses peroxisome proliferator-activated receptor-γ and attenuates pulmonary fibrosis. Br J Pharmacol. 2022;179:1304–18.
43. Bian EB, Zhao B, Huang C, Wang H, Meng XM, Wu BM, et al. New advances of DNA methylation in liver fibrosis, with special emphasis on the crosstalk between microRNAs and DNA methylation machinery. Cell Signal. 2013;25:1837–44.
44. Zeybel M, Hardy T, Wong YK, Mathers JC, Fox CR, Gackowska A, et al. Multigenerational epigenetic adaptation of the hepatic wound-healing response. Nat Med. 2012;18:1369–77.
45. Hardy T, Zeybel M, Day CP, Dipper C, Masson S, McPherson S, et al. Plasma DNA methylation: a potential biomarker for stratification of liver fibrosis in non-alcoholic fatty liver disease. Gut. 2017;66:1321–8.
46. Chen X, Li WX, Chen Y, Li XF, Li HD, Huang HM, et al. Suppression of SUN2 by DNA methylation is associated with HSCs activation and hepatic fibrosis. Cell Death Dis. 2018;9:1021.
47. Feng Y, Li Y, Jiang W, Hu Y, Jia Y, Zhao R. GR-mediated transcriptional regulation of m(6)A metabolic genes contributes to diet-induced fatty liver in hens. J Anim Sci Biotechnol. 2021;12:117.
48. Pan X, Bi Y, Cheng M, Qian Z, Wang L, You H, et al. METTL3 facilitates hepatic fibrosis progression via m6A-YTHDF2 dependent silencing of GPR161. BioRxiv. 2021. https://doi.org/10.1101/2021.12.15.472749.
49. Li Y, Kang X, Zhou Z, Pan L, Chen H, Liang X, et al. The m(6)A methyltransferase Mettl3 deficiency attenuates hepatic stellate cell activation and liver fibrosis. Mol Ther. 2022;S1525-0016:00441–5.
50. Zhang J, Bai R, Li M, Ye H, Wu C, Wang C, et al. Excessive miR-25-3p maturation via N(6)-methyladenosine stimulated by cigarette smoke promotes pancreatic cancer progression. Nat Commun. 2019;10:1858.
51. Wang S, Gan M, Chen C, Zhang Y, Kong J, Zhang H, et al. Methyl CpG binding protein 2 promotes colorectal cancer metastasis by regulating N(6)-methyladenosine methylation through methyltransferase-like 14. Cancer Sci. 2021;112:3243–54.
52. Wu S, Zhang L, Deng J, Guo B, Li F, Wang Y, et al. A novel micropeptide encoded by Y-linked LINC00278 links cigarette smoking and AR signaling in male esophageal squamous cell carcinoma. Cancer Res. 2020;80:2790–803.

ACKNOWLEDGEMENTS

This work was supported by the National Natural Science Foundation of China (32272962, 31972638), and the Priority Academic Program Development of Jiangsu Higher Education Institutions.

AUTHOR CONTRIBUTIONS

RZ and YF formulated the idea and designed the experiments. YF, SG and YZ performed and analyzed most of the experiments. HD and YH helped with animal work and provided technical help. JQ, LW and YJ performed some experiments and helped with data analysis. RZ and YF wrote the manuscript.

COMPETING INTERESTS

The authors declare no competing interests.

ETHICAL APPROVAL

The animal experiment was approved by the Animal Ethics Committee of Nanjing Agricultural University. The sampling procedure followed the "Guidelines on Ethical Treatment of Experimental Animals" (2006) No. 398 set by the Ministry of Science and Technology, China.

ADDITIONAL INFORMATION

Supplementary information The online version contains supplementary material available at https://doi.org/10.1038/s41418-023-01130-3.

Correspondence and requests for materials should be addressed to Ruqian Zhao.

Reprints and permission information is available at http://www.nature.com/reprints

Publisher's note Springer Nature remains neutral with regard to jurisdictional claims in published maps and institutional affiliations.